

# Identification of Piezoelectric Actuator Using Bayesian Approach and Neural Networks

Lenka Kuklišová Pavelková<sup>a</sup> and Květoslav Belda<sup>b</sup>

*Department of Adaptive Systems,  
The Czech Academy of Sciences, Institute of Information Theory and Automation,  
Pod Vodárenskou věží 4, CZ-182 00, Prague 8, Czech Republic*

**Keywords:** Piezoceramic Actuator, Hammerstein Model, Hysteresis, ARX Model, Bounded Noise, Bayesian Estimation, Physical Modelling, Continuum Mechanics, Euler–Bernoulli Beam Theory.

**Abstract:** The paper deals with a modelling and identification of a class of piezoelectric actuators intended for mechatronic and bio-inspired robotic applications. Specifically, a commercial piezoelectric bender PL140 from Physik Instrumente Co. is used. Considering catalogue/datasheet parameters, a physical model of PL140 is derived using Euler-Bernoulli beam theory. This model serves as a substitution of reality to generate proper data without potentially damaging the real actuator. However, due to its complex structure, this model cannot be used for control design. For this purpose, a Hammerstein model is proposed. It consists of a static nonlinear part describing the hysteresis and a dynamic linear part that is represented by the auto-regressive model with exogenous input (ARX model). The nonlinear part of the Hammerstein model is identified by a neural network. The Bayesian approach is used for the estimation of the ARX model parameters.

## 1 INTRODUCTION

Continuous progress in science and technology stimulates the demand for novel materials and devices. Piezoelectric actuators represent such a device. They have great potential in various fields such as micro-robotics, precision instruments or biomedicine (Gao et al., 2024).

Piezoelectric actuator (PEA) uses electro-mechanical coupling (inverse piezoelectric effect) to convert input electrical energy into output force or motion. Piezoelectric materials can be classified into single crystals, piezoelectric ceramics (PZT) and polymers. For a precision positioning, PZT is mostly used (Zhou et al., 2024). However, the accuracy of the generated motion is significantly impacted by the intrinsic non-linearity of PEAs under dynamic working conditions. This non-linearity arises mainly from hysteresis. Therefore, suitable modeling approaches that are able to model this nonlinearity are required to achieve higher motion accuracy (Kanchan et al., 2023).


The mechanical behavior of materials can be modelled by means of continuum mechanics. Never-

theless, the respective partial differential equations are too complex to be solved analytically. Therefore, a numerical technique called the finite element method (FEM) is used to solve these equations for complex systems in a computationally feasible manner (Hughes, 2003). However, the obtained model is still too complex for the control tasks. Thus, alternative models are used for nonlinear modeling of PZT actuators. They incorporate a black-box modeling together with a physical understanding of the hysteretic system (Ismail et al., 2009).

A hysteresis can be modelled either by using operator superposition or by differential equations (Dai et al., 2023). In the context of piezo actuators, the Bouc-Wen (BW) model, which belongs to the second group, is often used (Ismail et al., 2009).

However, the BW model only provides a static description, so it is often supplemented with a dynamic linear part such as auto-regressive model with exogenous input (ARX model). This combination of static non-linear and dynamic linear parts corresponds to the concept of Hammerstein's model (Dai et al., 2023).

Currently, the required control model is also often identified by artificial neural networks (ANNs) (Uralde et al., 2023).

<sup>a</sup>  <https://orcid.org/0000-0001-5290-2389>


<sup>b</sup>  <https://orcid.org/0000-0002-1299-7704>



Figure 1: PEA bender PL140.

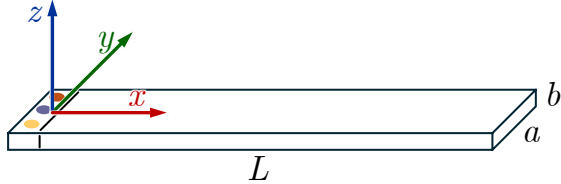


Figure 2: Main dimensions of PEA bender PL140.

This paper aims to provide a nonlinear data-driven model of the commercial piezoelectric bender PL140 of Physik Instrumente (PI) Co. The model is intended for a subsequent use in the micro-position control tasks. The proposed model will be based on a Hammerstein model.

Simultaneously, a physically based model is developed as a substitute of the real piezo bender. It is meant to simulate data for the identification of the above mentioned data-driven model without the need for an actual piezoelectric actuator.

The paper is organized as follows. In Section 2, a physical model of the piezoelectric bender PL140 is introduced. In Section 3, a relevant data-driven model is presented and the estimation of its parameters is proposed. The simulation experiments using both physical and data-driven models are described in Section 4.

## 2 PHYSICAL MODEL

This section summarises physical model of the PEA including the related theory. Namely the PICMA Bender PL140 is considered, see Figure 1. The simulation model is realized using MATLAB/Simulink environment and serves as a substitute for the real PEA.

### 2.1 Beam Theory for Piezo Bender

Physical bodies can be described using the general theory of continuum mechanics (Bruno et al., 2018). In the case of a prism-shaped piezo bender, i.e. a beam, a simplification in the form of Euler-Bernoulli beam theory can be used (Tadmor and Kósa, 2003). This theory will be considered and applied to model construction in this section. The obtained model is considered as a model substitut-

ing a real piezo ceramic beam. We consider that used piezo bender actuator is built from a homogeneous isotropic linear elastic piezoceramic material. Its stress  $\sigma$  is related to the strain  $\varepsilon$  by  $\sigma = E\varepsilon$ , where  $E$  is the Young's modulus. Then, general constitutive equations (Bruno et al., 2018) considering strains in space are as follows

$$\sigma = C\varepsilon - e^T E_o \quad (1)$$

$$d = e\varepsilon + \epsilon E_o \quad (2)$$

where  $E_o$ ,  $C$ ,  $\varepsilon$ ,  $e$ ,  $d$  and  $\epsilon$  are the electric field, compliance tensor, strain field, electric displacement field, piezo stress coefficient tensor and permittivity tensor at constant or zero strain, respectively. The required beam equations can be separated from (1) and (2). Let us proceed from strain along axis  $x$  (simplifying a general three-dimensional problem to a one-dimensional one,  $\circ \rightarrow (x \wedge z)$ , i.e. corresponding directions):

$$\varepsilon \rightarrow \varepsilon_{xx}(x, z) = -z \frac{d\varphi_y}{dx}(x) \quad (3)$$

$$E_o \rightarrow E_z = \frac{u}{b} \quad (4)$$

$$\sigma \rightarrow \sigma_{xx}(x, z) = -c_{11} z \frac{d\varphi_y}{dx}(x) - e_{31} \frac{u}{b} \quad (5)$$

where  $c_{11} = E$  and  $E_z$  is electric field perpendicular to plane  $xy$  and  $u$  is input voltage between surface electrodes of PEA. Then, bending moment from the stress field is

$$M_y(x) = - \iint z \sigma_{xx}(x, z) dS \quad (6)$$

By performing a double integral in (6), the bending moment is expressed as follows

$$M_y(x) = EI \frac{d\varphi_y}{dx}(x) + abe_{31}u \quad (7)$$

where  $I = \frac{1}{12}ab^3$  is the second moment of area of the rectangular cross-section.

Let us continue by developing the equation for electric displacement (2), again simplifying to the relevant one-dimensional subspace, as:

$$d_z(x, z) = e_{31} \varepsilon_{xx}(x, z) + \epsilon E_z \quad (8)$$

$$d_z(x, z) = -e_{31} z \frac{d\varphi_y}{dx}(x) + \epsilon \frac{u}{b} \quad (9)$$

$$dq = \iint d_z dS = e_{31} a b d\varphi_y \quad (10)$$

where  $dq$  is infinitesimal accumulated charge at a bend characterized by a bend angle change.

Thus, the charge  $q$  for a specific bend can be expressed as follows

$$q = e_{31} ab (\varphi_y(x_{k+1}) - \varphi_y(x_k)) \quad (11)$$

Then, the resulting Euler-Bernoulli beam equations for torque and charge are as follows

$$M_y(x) = EI \frac{d^2\varphi_y}{dx^2}(x) + ab e_{31} u \quad (12)$$

$$q = e_{31} ab (\varphi_y(x_{k+1}) - \varphi_y(x_k)) + \frac{\epsilon a \ell}{b} u \quad (13)$$

The set of equations (7)-(13) leads to the state-space finite-element form (16) of one element of the modelled beam divided into  $n$  elements:

$$\begin{bmatrix} F_C \\ \tau_C \\ F_R \\ \tau_R \end{bmatrix} = K \begin{bmatrix} z_C \\ \varphi_C \\ z_R \\ \varphi_R \end{bmatrix} \quad (14)$$

$$\begin{bmatrix} \bar{M} & 0 \\ 0 & 0 \end{bmatrix} \begin{bmatrix} \ddot{x} \\ 0 \end{bmatrix}$$

$$+ \begin{bmatrix} K & v_{\text{piezo}} \\ -v_{\text{piezo}}^T & \delta_{\text{piezo}} \end{bmatrix} \begin{bmatrix} x \\ u \end{bmatrix} = \begin{bmatrix} f \\ q \end{bmatrix} \quad (15)$$

where

$$K = \frac{EI}{\ell^3} \begin{bmatrix} 12 & 6\ell & -12 & 6\ell \\ 6\ell & 4\ell^2 & -6\ell^2 & 2\ell^2 \\ -12 & -6\ell & 12 & -6\ell \\ 6\ell & 2\ell^2 & -6\ell & 4\ell^2 \end{bmatrix}$$

$$\bar{M} = \frac{m}{420} \begin{bmatrix} 156 & 22\ell & 54 & -13\ell \\ 22\ell & 4\ell^2 & 13\ell & -3\ell^2 \\ 54 & 13\ell & 156 & -22\ell \\ -13\ell & -12\ell & -22\ell & 4\ell^2 \end{bmatrix}$$

$$v_{\text{piezo}} = [0 \quad e_{31} ab \quad 0 \quad -e_{31} ab]^T$$

$$\delta_{\text{piezo}} = \frac{\epsilon a \ell}{b}$$

with added dumping matrix  $B$ , the final form is

$$M \begin{bmatrix} \ddot{x} \\ 0 \end{bmatrix} + B \begin{bmatrix} \dot{x} \\ 0 \end{bmatrix} + \bar{K} \begin{bmatrix} x \\ u \end{bmatrix} = \begin{bmatrix} f \\ q \end{bmatrix} \quad (16)$$

where  $m = \rho abl$  is the element mass with density  $\rho$  and  $\ell$  as element length and  $L = n\ell$  total beam length,  $a$  and  $b$  are cross-sectional parameters – width and thickness respectively (see Figure 2),  $x = [z_C \varphi_C z_R \varphi_R]^T$  is generalized coordinate vector,  $e_{31}$  is a piezoelectric stress-charge coupling element and  $\epsilon$  is electrical permittivity.

The set (16) can be numerically solved in  $n$ -element chain, where terms  $K$ ,  $M$ ,  $B$  (= zero matrix but  $b_{11} \neq 0$ ),  $q$  and  $f = [F_C \tau_C F_R \tau_R]^T$  are stiffness matrix, mass matrix, stiffness finite element matrix, damping matrix, accumulated charge through PEA and generalized force effects, respectively, with right dimensions (Benjeddou et al., 1997).

The relations between available datasheet parameters and material parameters, which can be equally used in the equations and MATLAB/Simulink/Simscape blocks for Piezo Bender simulation, are summarised as follows (Tadmor and Kósa, 2003)

$$e_{31} = -\frac{2\ell F_{\text{block}}}{3ab u_{\text{rated}}} \quad (17)$$

$$E = -\frac{4F_{\text{block}} \ell^3}{y_{\text{free}} ab} \quad (18)$$

$$\epsilon = \frac{b}{a\ell} \left( C_{\text{piezo}} + \frac{4F_{\text{block}} y_{\text{free}}}{y_{\text{free}} ab^3} \right) \quad (19)$$

where parameters on the right side of equations:  $F_{\text{block}}$ ,  $a$ ,  $b$ ,  $u_{\text{rated}}$ ,  $y_{\text{free}}$  and  $C_{\text{piezo}}$  – blocking force, dimensions, rated drive voltage and free deflection at  $u_{\text{rated}}$ , beam capacitance, respectively – can be found in specific datasheet of PI Co.

The following section will focus on the modelling based on Simulink block models that can consider both the parameter types above.

## 2.2 Simscape Model

In the context of physical analysis above, to construct a suitable simulation model representing a real beam, MATLAB/Simulink with Simscape block libraries offers a simple start (user-friendly pre-arranged alternative to programming the mathematical equations defined in Section 2.1) for experimental research and development, see Figure 3. This model has several advantages such as structural clarity, fast implementation considering real physical parameters and constants contained in data sheets of producers.

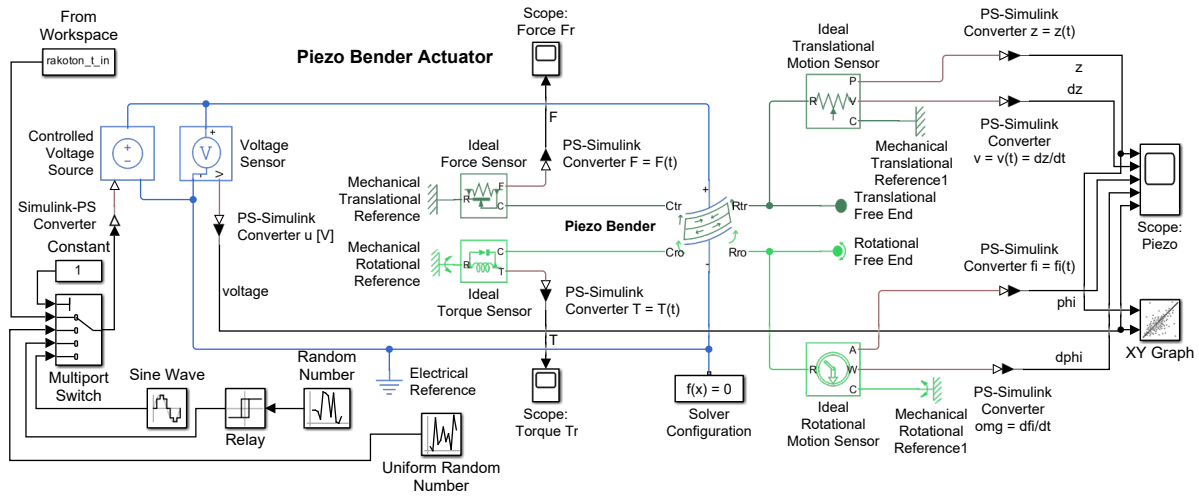


Figure 3: Simulink model comprising Simscape blocks.

The Simulink model can be described as follows. The main block is Piezo Bender block (MathWorks, 2021). It represents piezoelectric bimorph beam of rectangular cross-section that is connected trough mechanical translational and rotational reference via ideal force and torque sensors to the ground on one side and on other side leaved free via translational and rotational free ends. They are connected with ideal translational and rotational motion sensors. Input voltage of PEA is provided by controlled voltage source.

The function of Piezo bender block is as follows: it bends when an electrical potential is applied across its layers. Conversely, when a piezo bender is bended, it generates an electrical potential.

various control algorithms and simulation tools (Gao et al., 2015).

A block diagram of the model is shown in Figure 4. The block NLS describes the rate-independent (static) hysteresis nonlinearity and the block LD describes rate-dependent (dynamic) linear part characteristic of the piezoelectric actuator. The involved signals  $u_t$ ,  $z_t$ ,  $v_t$ , and  $y_t$  represents an input, hidden unmeasurable variable, noise, and output, respectively;  $t \in \{1, 2, \dots, \bar{t}\}$  denotes a discrete time.

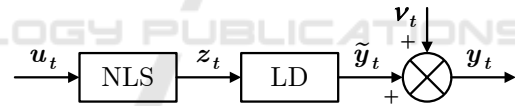


Figure 4: Block diagram of Hammerstein model

### 3 DATA DRIVEN MODEL

This section presents a data-driven model of the piezo bender PL140 that is aimed to be used in microposition control tasks.

#### 3.1 Hammerstein Model

The Hammerstein model describes a dynamics of nonlinear systems by combining a static nonlinearity followed by a linear dynamic model. In the context of PEA, it concatenates various basic (static) hysteresis models with dynamic transfer functions, giving the model better dynamic description ability (Dai et al., 2023). Using the Hammerstein model for a description of a PZT actuator simplifies the analysis because it separates the nonlinear hysteresis component from the linear dynamic behavior. It is also easy to use in a

Generally, there is a coupling between the linear part and the nonlinear part of Hammerstein model. Nevertheless, under certain conditions, the linear part can be separated from the nonlinear one during the identification.

The paper (Bai, 2004) proposes such an identification algorithm. In the first step, the system is excited by the pseudo-random binary sequences (PRBS) input. Under this input, the nonlinearity will not appear as it is not excited. Then,  $z_t = u_t$  and the linear part LD can be identified independently of the non-linear one.

On the other side, to identify the nonlinear part NLS, the input has to be sufficiently rich. Therefore, a new input–output data set  $\{u_t, y_t\}$  needs to be generated. We consider that NLS is unknown but static. Therefore, if  $u_t$  and  $z_t$  are available (see Figure 4), the structural information on the unknown

NLS can be derived from their graphical representation (Bai, 2004). We will estimate the unmeasurable  $z_t$  using the mentioned rich input–output data set and already identified linear part LD.

### 3.2 Uniform ARX Model

The LD part of Hammerstein model (Figure 4) is often represented by an ARX model (Dai et al., 2023). Here, we will consider the ARX model with an additive bounded noise, as it is suitable for real application (d’Onofrio, 2013). Namely, we will consider a uniformly distributed noise. When considering a model with uniform noise, we do not need to know the statistical properties of the noise, but only its bounds.

The ARX model with a uniform noise is defined as follows

$$y_t = \psi_t^T \theta + \nu_t, \quad \nu_t \sim \mathcal{U}_\nu(-r, r) \quad (20)$$

where

$y_t$  is an observable output,

$u_t$  is an optional known input,

$\psi_t$  is a finite-dimensional regression vector,

$$\psi_t = [y_{t-1}, \dots, y_{t-m}, u_{t-1}, \dots, u_{t-m}]^T,$$

$\theta$  is a vector of unknown regression coefficients,

$$\theta = [a_1, \dots, a_m, b_1, \dots, b_m]^T, \quad m \text{ is model order,}$$

$T$  denotes the transposition,

$\nu_t$  is a uniformly distributed i.i.d. white noise, i.e., zero mean and uncorrelated with older observations,

$\mathcal{U}_\nu(-r, r)$  denotes a uniform distribution of  $\nu$ ;  $r > 0$  is a noise range.

To estimate the regression coefficients of ARX model (20), we use the Bayesian framework (Kárný et al., 2006). There, a system of interest is described by the following probability density functions (pdfs):

$$\begin{aligned} &\text{prior pdf } f(\Theta) \equiv f(\Theta|d(0)), \\ &\text{observation model } f(y_t|u_t, d(t-1), \Theta), \end{aligned} \quad (21)$$

where  $\Theta$  is an unknown parameters vector.

Bayesian parameter estimation consists in the recursive evolution of the posterior pdf  $f(\Theta|d(t))$  that starts from the prior pdf  $f(\Theta)$ :

$$f(\Theta|d(t)) \propto f(y_t|u_t, d(t-1), \Theta) f(\Theta|d(t-1)) \quad (22)$$

where  $d(t) = [d_t, d_{t-1}, \dots, d_1]$ ,  $t = 1, 2, \dots, \bar{t}$ , is a sequence of observed data records,  $d_t = (y_t, u_t)$ ,  $\propto$  means the equality up to the normalising constant. Note that here is no formal distinction of a random variable, its realization and pdf argument.

Considering the ARX model (20) in the role of the observation model (21) with  $\Theta$  comprising both

$\theta$  and  $r$ , then the use of (22) leads to the increasing complexity of the support of  $f(\Theta|d(t)) \equiv f(\Theta|\psi_t)$ . In (Pavelková and Kárný, 2012), the approximate estimation is proposed that recursively circumscribe this complex support by a feasible set. The following expected values of both the model parameters  $\theta$  and the noise bound  $r$  are provided:

$$\hat{\theta} = \hat{r} v_\psi^{-1} [l_{n-1}, 0] \frac{u+l}{2} - v_\psi^{-1} v_y, \quad (23)$$

$$v = \begin{bmatrix} v_\psi & v_y \\ 0 & 1 \end{bmatrix}$$

$$\hat{r} = \frac{\nu+1}{\nu} \frac{1-\gamma^\nu}{1-\gamma^{\nu+1}} u_n^{-1}, \quad \gamma = \frac{\max(l_n, 0)}{u_n}.$$

where  $\nu$  corresponds to the number of processed data,  $[l_{n-1}, 0]$  denote  $n-1$  rows of unit  $n$  matrix, column vectors  $l$ ,  $u$  and the square matrix  $v$  are the approximate statistics that define the approximate support  $\hat{S}_t$  of  $f(\Theta|d(t))$  as follows:

$$\hat{S}_t = \{\Theta : \Theta_n > 0, l \leq v \Theta \leq u\}, \quad (24)$$

$\Theta_n = 1/r$  is the  $n$ -th entry of the vector  $\Theta$ ,  $\Theta = [-\theta^T \Theta_n, \Theta_n]$ . The matrix  $v$  has the upper triangular form with unit diagonal.

The update of  $\hat{S}_t$  includes extension of  $v$  by one row corresponding to the vector  $\Psi_t = [\psi_t^T, y_t]$  and extension of  $l$  by  $-1$  and  $u$  by  $1$  followed by the orthogonal rotation that zeroes the last rows of  $l$ ,  $v$ ,  $u$  and keep the triangular form of  $v$  (Pavelková and Kárný, 2012).

Note that we do not need to know the noise range  $r$  because it is estimated together with the model parameters.

### 3.3 Static Nonlinearity

To identify NLS, the static nonlinear part of the Hammerstein model, we need a data set of  $u_t$  and  $z_t$ , see Figure 4. The inputs  $u_t$  are available. The hidden variables  $z_t$  can be estimated using the inverse estimated ARX model representing LD part and from the known  $y_t$  generated by the Simscape model, Figure 3. Considering that LD is represented by the ARX model (20), the inverse model with input  $y_t$  and output  $z_t$  has the following form:

$$\begin{aligned} z_t &= \hat{z}_t - \frac{1}{b_1} v_{t+1} = \\ &= \frac{1}{b_1} (y_{t+1} - a_1 y_t - \dots - a_m y_{t-m+1} - \\ &\quad - b_2 z_{t-1} - \dots - b_m z_{t-m+1}) - \frac{1}{b_1} v_{t+1} \end{aligned} \quad (25)$$

where  $a_i, b_i, i = 1, 2, \dots, m$ , corresponds to the parameters of the ARX model (20). Considering the noise  $v_{t+1}, z_t$  is uniformly distributed on the support  $[\hat{z}_t - r/b_1, \hat{z}_t + r/b_1]$  with the mean  $\hat{z}_t$ .

To identify the NLS block of Hammerstein model, we use the generated inputs  $u_t$  together with estimated means  $\hat{z}_t$  of hidden variable  $z_t$  (25). As a mapping function, a neural network *idNeuralNetwork* from MATLAB was chosen. This function is designed to identify nonlinear ARX models and Hammerstein-Wiener models and requires Statistics and Machine Learning Toolbox or Deep Learning Toolbox (MathWorks, 2023).

Mathematically, *idNeuralNetwork* is a function that maps vector of regressors  $X_t$  to a single scalar output  $y_t$  using the relationship

$$y_t = S(X_t^T Q) \quad (26)$$

where  $X_t = [\psi_1^T, \dots, \psi_t^T]^T$ ,  $Q$  is a projection matrix,  $S(\cdot)$  represents a neural network object. This object is defined by the number of hidden layers including number of nodes and activation function for each layer.

### 3.4 Identification Procedure

Consider the Hammerstein model in Figure 4. Then, the identification of data-driven model of PL140 is as follows:

- generate PRBS data using Simscape model depicted in Figure 3
- estimate the parameters of the block LD in Hammerstein model represented by the ARX model (20) according to (23) using the generated PRBS data
- generate new rich data (with sin waveform, random or (Rakotondrabe, 2021) inputs)
- estimate the  $z_t$  in Hammerstein model as the output of inverse ARX model (25) where the generated outputs  $y_t$  from c) serve as inputs
- identify the NLS block in Hammerstein model as described in Subsection 3.3 using input data  $u_t$  from c) and output data  $\hat{z}_t$  from d) together with the mapping function (26)
- generate new rich data set as described in c) to test the identified Hammerstein model accuracy.

## 4 EXPERIMENTS

This section presents a performance of the proposed identification scheme, Subsection 3.4, applied to the piezoelectric bender PL140.

The real-like data are generated by the Simscape model of piezoelectric bender PL140, see Figure 3. The following input sources corresponding the applied voltage are available:

PRBS - pseudorandom binary sequence with parameter  $C_P$ , i.e. sequence of random numbers from the set  $\{-C_P, C_P\}$

RAND - data uniformly distributed within a given interval  $[-C_R, C_R]$

SINE - sine wave signal of tunable amplitude and frequency

RAKO - input data from the Matlab example ‘‘Piezoelectric Actuator Model Identification Using Machine Learning’’ (Rakotondrabe, 2021)

The experiments were performed in accordance with the proposed identification scheme (Subsection 3.4) with the sampling frequency  $T_s = 10^{-3}$  s.

First, the PRBS data with  $C_P = 1$  were generated and subsequently used to estimate the parameters of the ARX model (20). The time course of the regression coefficients estimates are depicted in Figures 5 – 8. It can be seen that although the estimates converge to a particular values, they do not stabilize and oscillate around these values.

For further use, we set the point parameter estimates as the mean values from the steady-state part of the relevant time courses. The estimates are shown in the Table 1.

Table 1: Point estimates of the ARX model (20).

$a_1$	$a_2$	$b_1$	$b_2$
1.1980	-0.9719	0.0042	0.0021

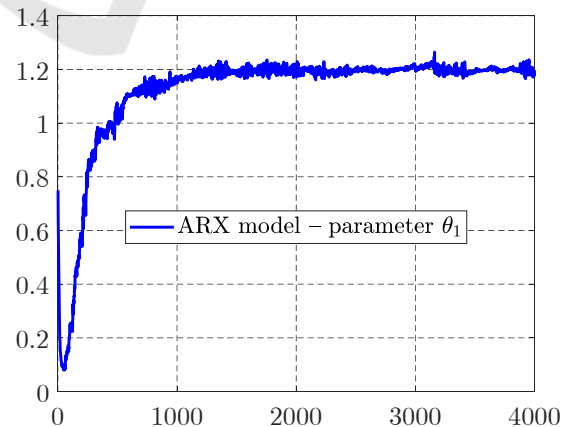


Figure 5: Time course (in  $10^{-3}$  s) of the parameter estimate  $\theta_1 = a_1$  in ARX model (20).

Then, the new input-output data with SINE input was generated to be used for estimating the hidden

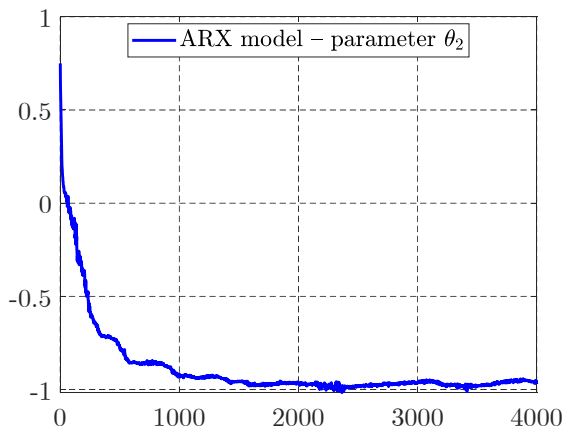


Figure 6: Time course (in  $10^{-3}$  s) of the parameter estimate  $\theta_2 = a_2$  in ARX model (20).

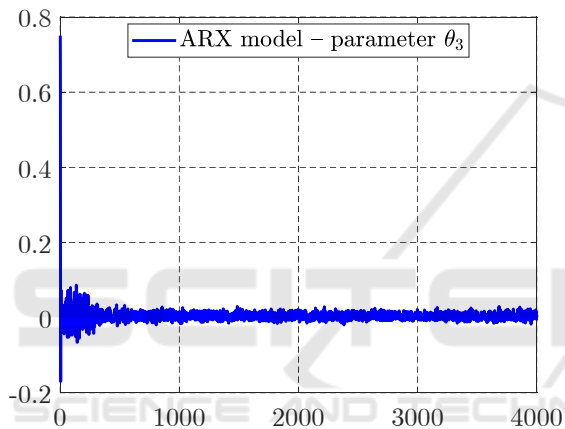


Figure 7: Time course (in  $10^{-3}$  s) of the parameter estimate  $\theta_3 = b_3$  in ARX model (20).

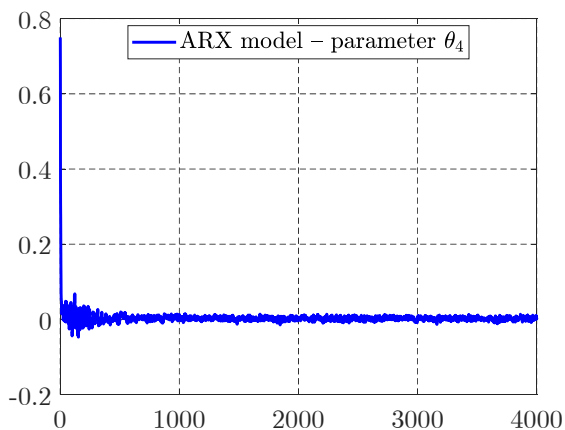


Figure 8: Time course (in  $10^{-3}$  s) of the parameter estimate  $\theta_4 = b_4$  in ARX model (20).

variable  $z_t$  and the subsequent identification of the nonlinear part NLS represented by (26). In the experiment, we have used neural network with three hid-

den layers and the hyperbolic tangent activation function. Model parameters were obtained using the Matlab function *nlrx*. The estimated hysteresis curve, i.e. relationship between the applied input voltage  $u$  and the mean of the hidden variable  $\hat{z}$  is depicted in Figure 9.

To test the performance of identified Hammerstein model, we generated another rich input-output data sets with RAND inputs and used them for the prediction task. A sample example of the simulated outputs and their predictions is shown in Figure 10.

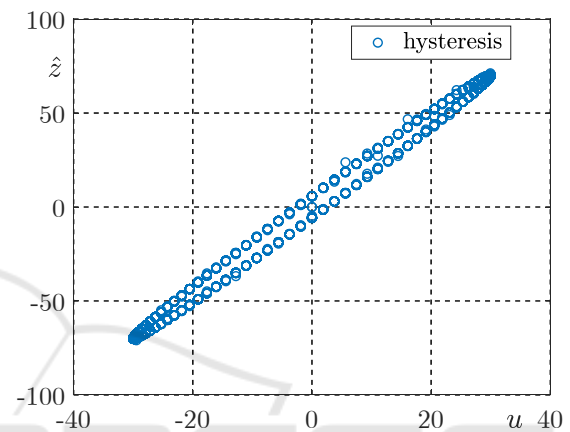


Figure 9: NLS part of Hammerstein model – identified hysteresis between  $u$  and  $\hat{z}$ .

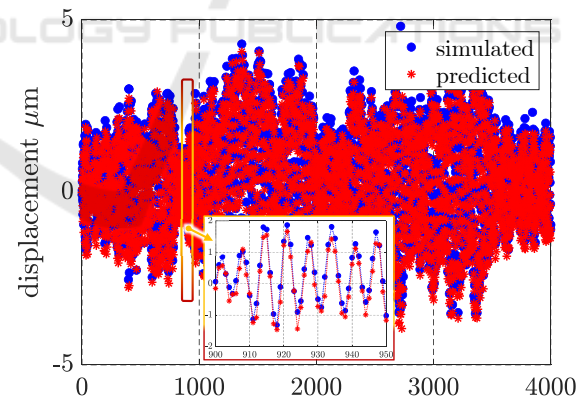


Figure 10: Time course (in  $10^{-3}$  s) of predicted (red) and simulated (blue) outputs with a zoomed part for the Hammerstein model excited by random inputs.

## 5 CONCLUSION

This paper deals with the construction of a physical model of the commercial piezoelectric bender PL140 as well as with the identification of the corresponding data-driven model. Nevertheless, the presented results can be easily adapted to other beam PZT actua-

tors. The explanation of these models provides interested readers with the necessary background to carry out their own experiments.

The Simscape model is based on a physical analysis and it is intended as a substitute for the real piezoelectric actuator. It serves as an experimental data source. It has the advantage that various experiments can be performed without expensive measuring equipment and without the risk of damaging the real actuator.

The identified data-driven model is intended for a subsequent model-based micro-positioning control design. This control design will be tuned on the developed Simulink model and then verified on a real bender PL140.

The used identification scheme, i.e. Hammerstein model, with an independent estimation of the linear dynamic and the nonlinear static parts, offers freedom in the choice of both the linear model and a function representing the nonlinear static part.

Our choice of uniform ARX model was motivated by the facts that models with a bounded noise are suitable for a real applications, and that the estimation algorithm is simple and not time-consuming. Moreover, we do not need to know the noise bound  $r$ , because it is estimated together with the model parameters.

A function representing the nonlinear static part was conveniently identified by the means of a neural network MATLAB toolbox.

The proposed model offers a good prediction results with isolated outliers. The achieved result could be further improved by tuning the network parameters. Another increase in model accuracy can be achieved by a creep modelling. After hysteresis, the creep is another factor responsible for nonlinearity in the piezoelectric actuator. It is a time-dependent effect that causes a slow drift of the output displacement when the input voltage changes suddenly (Kanchan et al., 2023).

Future research will focus on incorporating the proposed data-driven model into a model predictive control task and on a testing the developed algorithms on a real piezo actuator.

## ACKNOWLEDGEMENTS

This work was supported by The Czech Academy of Sciences, Institute of Information Theory and Automation under the project No. 23-04676J of the Czech Science Foundation: Controllable Gripping Mechanics: Modelling, Control and Experiments.

## REFERENCES

- Bai, E.-W. (2004). Decoupling the linear and nonlinear parts in Hammerstein model identification. *Automatica*, 40(4):671–676.
- Benjeddou, A., Trindade, M. A., and Ohayon, R. (1997). A unified beam finite element model for extension and shear piezoelectric actuation mechanisms. *Journal of Intelligent Material Systems and Structures*, 8(12):1012–1025.
- Bruno, B. P., Fahmy, A. R., Stürmer, M., Wallrabe, U., and Wapler, M. C. (2018). Properties of piezoceramic materials in high electric field actuator applications. *Smart Materials and Structures*, 28(1):015029.
- Dai, Y., Li, D., and Wang, D. (2023). Review on the nonlinear modeling of hysteresis in piezoelectric ceramic actuators. *Actuators*, 12(12).
- d’Onofrio, A. (2013). *Bounded Noises in Physics, Biology, and Engineering*. Springer.
- Gao, T., Liao, Q., Si, W., Chu, Y., Dong, H., Li, Y., Liao, Y., and Qin, L. (2024). From fundamentals to future challenges for flexible piezoelectric actuators. *Cell Reports Physical Science*, 5(2):101789.
- Gao, X., Ren, X., Zhu, C., and Zhang, C. (2015). Identification and control for Hammerstein systems with hysteresis non-linearity. *IET Control Theory & Applications*, 9(13):1935–1947.
- Hughes, T. J. (2003). *The finite element method: linear static and dynamic finite element analysis*. Courier Corporation.
- Ismail, M., Ikhouane, F., and Rodellar, J. (2009). The hysteresis Bouc-Wen model, a survey. *Archives of computational methods in engineering*, 16:161–188.
- Kanchan, M., Santhya, M., Bhat, R., and Naik, N. (2023). Application of modeling and control approaches of piezoelectric actuators: A review. *Technologies*, 11(6):155.
- Kárný, M., Böhm, J., Guy, T. V., Jirsa, L., Nagy, I., Nedoma, P., and Tesař, L. (2006). *Optimized Bayesian Dynamic Advising: Theory and Algorithms*. Springer, London.
- MathWorks (2021). Piezo bender. [www.mathworks.com/help/sps/ref/piezobender.html](http://www.mathworks.com/help/sps/ref/piezobender.html). Accessed: 2024-06-30.
- MathWorks (2023). Available mapping functions for nonlinear ARX models. [www.mathworks.com/help/ident/ref/idneuralnetwork.html](http://www.mathworks.com/help/ident/ref/idneuralnetwork.html). Accessed: 2024-06-30.
- Pavelková, L. and Kárný, M. (2012). Approximate Bayesian recursive estimation of linear model with uniform noise. *IFAC Proceedings Volumes*, 45(16):1803–1807.
- Rakotondrabe, M. (2021). Piezoelectric actuator model identification using machine learning. [www.mathworks.com/help/ident/ug/machine-learning-based-identification-of-piezoelectric-actuator.html](http://www.mathworks.com/help/ident/ug/machine-learning-based-identification-of-piezoelectric-actuator.html). Accessed: 2024-02-08.
- Tadmor, E. B. and Kósa, G. (2003). Electromechanical coupling correction for piezoelectric layered beams. *Journal of Microelectromechanical Systems*, 12(6):899–906.



- Uralde, J., Artetxe, E., Barambones, O., Calvo, I., Fernandez-Bustamante, P., and Martin, I. (2023). Ultra-precise controller for piezoelectric actuators based on deep learning and model predictive control. *Sensors*, 23(3).
- Zhou, X., Wu, S., Wang, X., Wang, Z., Zhu, Q., Sun, J., Huang, P., Wang, X., Huang, W., and Lu, Q. (2024). Review on piezoelectric actuators: materials, classifications, applications, and recent trends. *Frontiers of Mech. Engin.*, 19(1):6.

